




Observation of a fission mode with very short elongation for the neutron-rich ^{257}Md nucleus at high excitation energy

A. Pal ¹, S. Santra ^{1,2,*}, P. C. Rout,^{1,2} Ramandeep Gandhi ¹, Abhijit Baishya ¹,
T. Santhosh ^{1,2}, R. Tripathi,^{2,3} and T. N. Nag^{2,3}

¹*Nuclear Physics Division, Bhabha Atomic Research Centre, Mumbai 400085, India*

²*Homi Bhabha National Institute, Anushaktinagar, Mumbai 400094, India*

³*Radio Chemistry Division, Bhabha Atomic Research Centre, Mumbai 400085, India*



(Received 14 July 2021; accepted 23 August 2021; published 23 September 2021)

Mass and total kinetic-energy (TKE) distributions of fission fragments from ^{257}Md nucleus populated by complete fusion of ^{19}F with ^{238}U have been measured in the range of excitation energy $E^* \approx 37\text{--}48$ MeV. Due to the skewness of the measured TKE distributions, two Gaussian distributions were required to explain the data. The events with high TKE must originate from the supershort mode of fission, the presence of which has been confirmed by measuring two additional reactions: $^{19}\text{F} + ^{232}\text{Th}$ and $^{18}\text{O} + ^{238}\text{U}$ involving first a different target and then a different projectile leading to compound nuclei ^{251}Es and ^{256}Fm , respectively, at similar excitation energies and comparing their mass-TKE correlation plots. The existence of considerable supershort mode of fission for the ^{257}Md nucleus up to $E^* \approx 48$ MeV, observed for the first time, reveals that such rare fission modes for neutron-rich exotic nuclei are far off from the liquid drop model predictions, even at high excitation energies.

DOI: [10.1103/PhysRevC.104.L031602](https://doi.org/10.1103/PhysRevC.104.L031602)

The process of nuclear fission is not only important for the existence of many transuranium nuclei and long-lived superheavy elements but also for the heavy-element formation in the astrophysical r process [1–4]. Recently, a lot of studies have been carried out on nuclear fission from heavy and superheavy elements [5–13], and also from the neutron-rich or neutron-deficient nuclei [14–20]. In general, the process is very different for different mass regimes. It is well studied that, for the mass region $200 < A < 226$, fission-fragment (FF) mass distributions are mainly symmetric whereas the contribution from asymmetric mode does not exceed 0.5% [21]. In contrast, for actinide nuclei with $A = 226\text{--}256$, the mass distribution is asymmetric for compound-nuclear excitation energy even up to ≈ 40 MeV. Interestingly, the FF mass distributions for the isotopes of Ra and Ac nuclei and the light isotopes of Th [22–24] are having comparable contributions from asymmetric and symmetric modes of fission. Most interestingly, the phenomenon of bimodal fission, where two modes with two different most probable total kinetic energies (TKEs) exist together are observed for the case of spontaneous and low-energy fission of neutron-rich nuclei in the region of Fm–Rf nuclei [25,26]. Here, the TKE distribution strongly differs from the Gaussian shape distribution, which is mostly found in the fission of other actinides. In general, several Gaussian functions representing different fission modes are required to describe the measured mass and TKE distributions. For instance, the TKE distribution from ^{258}Fm isotope [25] is described by sum of two Gaussian distributions: one peaking around 195 MeV and the other around 230 MeV,

corresponding to two distinct modes of fission, viz., asymmetric mode and a supershort mode, respectively. The two different modes of fission are understood to occur due to two different paths in the potential-energy surface undertaken by the compound nucleus as a function of deformation during the process of its evolution from compound nucleus formation up to the scission point. In one path (asymmetric mode), it reaches the scission point in a stretched neck configuration producing fission fragments with low TKE. But, in the second path (supershort), it reaches the scission point without any stretching, instead it reaches in a touching two-sphere configuration which results in higher Coulomb repulsion between two fragments, leading to a higher TKE.

Earlier it was known that bimodal fission appears for Fm isotopes ($Z = 100$) and more heavy elements when two fission fragments are close to the spherical proton $Z = 50$ and neutron $N = 82$ shell closures [13]. However, in a recent calculation [27] using four-dimensional Langevin approach it has been shown that bimodality actually starts appearing from the ^{254}Es nucleus where the symmetric mode makes a sudden transition from superlong to supershort fission mode.

To date, in the heavy-mass regions, the phenomenon of bimodality has been observed for the isotopes $^{258,259}\text{Fm}$, $^{259,260}\text{Md}$, $^{258,262}\text{No}$, $^{262,266,267}\text{Rf}$ [25,26], $^{267,268}\text{Db}$ [28], and $^{270,271}\text{Sg}$ [29] from either spontaneous fission or low-energy fission. Bimodality was also observed for $^{271,274}\text{Hs}$ [30] isotopes produced in heavy-ion-induced fusion reactions. It was shown that the supershort mode gradually disappears with increasing excitation energy of the compound nucleus and no contribution of this mode was observed beyond $E^* = 35$ MeV.

The theoretical work published in Ref. [27] suggests that supershort modes may be seen in much lighter nuclei ^{256}Fm

*ssantra@barc.gov.in

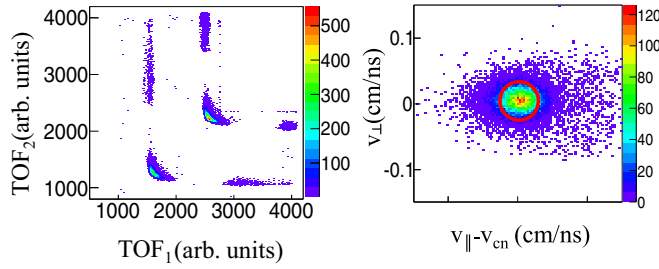


FIG. 1. Typical plots of (a) correlation of time of flights (TOF_1 vs TOF_2) of both fission fragments, cleanly identifying the binary fission events for both the beam pulses, and (b) $v_{\parallel} - v_{cn}$ versus v_{\perp} , obtained for $^{19}\text{F} + ^{238}\text{U}$ reaction at $E_{\text{beam}} = 98$ MeV. The area inside the red circle corresponds to the binary events following the complete fusion process.

and ^{254}Es . However, experimentally, so far contributions from supershort modes have been observed from nuclei only with $A > 257$. There is a measurement on ^{256}Fm [31] which does not report the presence of supershort modes. On the contrary, measurement of the ^{256}No [32] nucleus reports feeble contributions from that mode at high excitation energy. Therefore, measurements with $A = 256$ and 257 nuclei are very important to confirm the onset of the presence of the supershort mode.

In this Letter, we report the observation of bimodal fission from a nucleus ^{257}Md which lies in the boundary lines of nuclear chart showing bimodal fission. We also report for the first time the persistence of the supershort mode, even at excitation energy $E^* \approx 48$ MeV, which cannot be explained by the existing theoretical models.

Fission fragments have been measured for three reactions: $^{19}\text{F} + ^{238}\text{U}$, $^{18}\text{O} + ^{238}\text{U}$, and $^{19}\text{F} + ^{232}\text{Th}$ using pulsed beam of energies ranging from 80.9 to 98.0 MeV at the 14-UD BARC-TIFR Pelletron-Linac facility, Mumbai, India. A ^{238}U target of thickness $\approx 100 \mu\text{g}/\text{cm}^2$, sandwiched between two layers of ^{12}C of thickness $\approx 15 \mu\text{g}/\text{cm}^2$ each and a self-supporting ^{232}Th target of thickness $\approx 400 \mu\text{g}/\text{cm}^2$ were used. Two position-sensitive multiwire proportional chambers (MWPCs), each having an active area of $12.5 \text{ cm} \times 7.5 \text{ cm}$, were placed at folding angles at distances of 42.5 cm from the target center to detect the coincident fission fragments [33]. The detectors were placed symmetrically on either side of the beam direction, covering an angular range $\approx 72^\circ - 88^\circ$. The timing correlation spectrum of the two particles detected in coincidence, as shown in Fig. 1(a), provides a clean separation of the fission fragments from other elastic or quasi-elastic events. Position spectra were calibrated using the data with masks of known dimensions kept in front of the detectors, following which the values of scattering angle θ and azimuthal angle ϕ of the fission fragments were obtained on an event-by-event basis. Timing calibration was done using a precision time calibrator which generates two signals, one of which is used as a START and the other one as a STOP signal after providing a suitable delay. As described in Refs. [12,34], time zero was obtained by fulfilling the following criteria: (i) parallel component of velocity vector of the fissioning nucleus should be peaking at the velocity equal to the velocity of compound

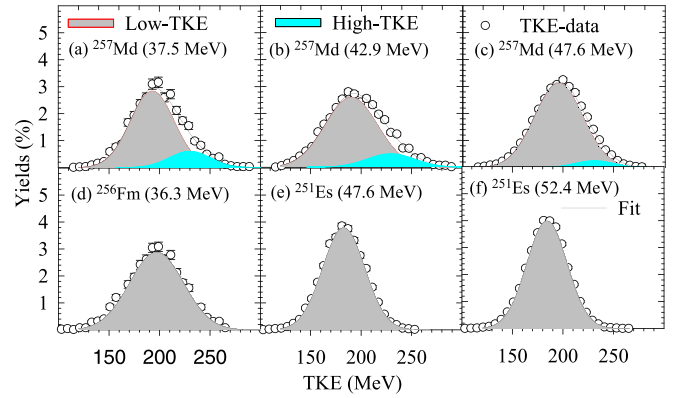


FIG. 2. Measured TKE distributions for (a)–(c) ^{257}Md , (d) ^{256}Fm , and (e), (f) ^{251}Es nuclei. TKE distributions shown in panels (a) and (b) were fit using two Gaussian distributions, in contrast to the others that were fit using single-Gaussian distribution.

nucleus and (ii) mass distribution which is obtained by taking the ratio of FF velocities ($v_{1c.m.}$, $v_{2c.m.}$) in the center-of-mass frame, should be symmetric around the half of the compound-nuclear mass. Energy loss in the target and backing medium has been calculated using the SRIM code [35] and has been taken into account in the above analysis. The target thickness being very small has negligible effect on the derived mass and TKE distributions.

In heavy-ion-induced reactions involving actinide targets, the probability of transfer-induced fission is quite significant for beam energies close to or below the Coulomb barrier. A correlation plot of parallel (v_{\parallel}) versus perpendicular (v_{\perp}) components of velocity vectors of fission fragments is very useful [11] to reject the contribution of transfer fission. A typical two-dimensional (2D) plot for $v_{\parallel} - v_{cn}$ versus v_{\perp} is shown in Fig. 1(b) for 98.0 MeV beam energy, where both v_{\perp} and $v_{\parallel} - v_{cn}$ for the majority of the events were observed at 0.0, which corresponds to a complete fusion reaction. The events within the red circle (of radius ≈ 0.02 cm/ns) in the above figure actually correspond to the binary events followed by complete fusion, and only these events have been analyzed to derive the mass and TKE distributions. The scattered events with v_{\parallel} larger (smaller) than the above radius have contribution from transfer-induced fission events at below (above) the barrier energy. The contribution of transfer fission within the red circle has been estimated from the three-Gaussian fit to the $v_{\parallel} - v_{cn}$ distribution and found to be very small ($\approx 2\% - 5\%$).

Using the measured velocities of the fission fragments and simple two-body kinematics, the masses and kinetic energies of the fragments have been determined event by event assuming that the sum of the projectile and target masses equals the compound-nuclear mass ($A_{CN} = A_P + A_T$). The TKE distributions of fission fragments produced from ^{257}Md nuclei for $E_{\text{beam}} = 87.1$, 93, and 98 MeV are shown by open circles in Figs. 2(a)–2(c). It can be observed that, for all the beam energies, the TKE distributions peak at energies close to 198 MeV, as expected from Viola systematics [36]. Due to the skewness in the shape of the TKE distributions, particularly for the first two energies (87.1 and 93.0 MeV), the best fit could only be achieved with two Gaussian distributions: one

TABLE I. Peak position P and width σ of the low- and high-TKE modes at different excitation energies observed for different reactions.

Nucleus	Reaction	E_{beam} (MeV)	E^* (MeV)	$P_{\text{low}}^{\text{TKE}}$ (MeV)	$\sigma_{\text{low}}^{\text{TKE}}$ (MeV)	$P_{\text{high}}^{\text{TKE}}$ (MeV)	$\sigma_{\text{high}}^{\text{TKE}}$ (MeV)
^{257}Md	$^{19}\text{F} + ^{238}\text{U}$	87.1	37.5	193.0	21.8	230.0	20.2
^{257}Md	$^{19}\text{F} + ^{238}\text{U}$	93.0	42.9	192.0	26.1	229.0	23.5
^{257}Md	$^{19}\text{F} + ^{238}\text{U}$	98.0	47.6	194.8	24.0	230.0	18.7
^{256}Fm	$^{18}\text{O} + ^{238}\text{U}$	80.9	36.2	196.9	26.6		
^{251}Es	$^{19}\text{F} + ^{232}\text{Th}$	93.0	47.6	182.7	21.0		
^{251}Es	$^{19}\text{F} + ^{232}\text{Th}$	98.0	52.4	184.2	19.9		

around 193 MeV and the other around 230 MeV, as shown by filled gray and cyan regions, respectively, in Figs. 2(a) and 2(b). It may be observed that in these two plots the peak corresponding to low TKE is much closer to the value obtained from the Viola systematics, whereas the peak corresponding to high TKE is possibly due to the supershort mode of fission, where large Coulomb repulsion between the two compact fragments is expected to generate higher TKE. At $E_{\text{beam}} = 98$ MeV [Fig. 2(c)], the TKE distribution shows a very small contribution from supershort mode, indicating the weakening of the supershort mode at higher beam energies.

To confirm that the above supershort mode observed in ^{257}Md , populated in the $^{19}\text{F} + ^{238}\text{U}$ reaction, is not due to some structure of the delivered pulsed beam or any target-related issues, the results have been compared with those obtained from the $^{19}\text{F} + ^{232}\text{Th}$ reaction at $E_{\text{beam}} = 93$ and 98 MeV, corresponding to $E^* = 47.6$ and 52.4 MeV where the TKE distributions were found to be perfectly Gaussian in shape, as expected [see Figs. 2(e) and 2(f)]. Furthermore, the results have been compared with another compound nucleus ^{256}Fm , populated in the $^{18}\text{O} + ^{238}\text{U}$ reaction, at $E_{\text{beam}} = 80.9$ MeV, corresponding to $E^* = 36.2$ MeV, the excitation-energy region where the supershort mode has been observed for the ^{257}Md nucleus. It was found that the TKE distributions for ^{256}Fm could also be fit by using a single-Gaussian function [see Fig. 2(d)], thereby confirming the presence of the supershort mode in the fission of the ^{257}Md nucleus. The details of the fitting parameters, including the peak positions and widths of low and high TKE distributions corresponding to different compound nuclei populated by different reactions, beam energies, and excitation energies, are listed in Table I.

The FF mass-TKE correlation plots are very useful in identifying different modes of fission such as asymmetric, superlong, and supershort modes of fission [27]. These correlation plots in the presence of the supershort mode of fission look distinctly different from those with its absence. The measured TKE distributions have already indicated the presence of bimodal fission in ^{257}Md nucleus. For further investigation, the correlation of the TKE with the mass of the fission fragments formed by the complete fusion of the target and projectile have been obtained for all energies, as shown for ^{257}Md [Figs. 3(a)–3(c)], ^{256}Fm [Fig. 3(d)], and ^{251}Es [Figs. 3(e) and 3(f)] nuclei. The events within the dotted rectangle, with TKE higher than 250 MeV, are in fact responsible for the skewness in the TKE distribution observed earlier and originate from the supershort mode. The nonobservation of any event within the dotted rectangles of Figs. 3(e) and 3(f) implies that ^{251}Es does

not exhibit the supershort mode of fission but only the standard asymmetric and superlong modes of fission. However, in Figs. 3(a)–3(c) corresponding to ^{257}Md , there are significant numbers of events with TKE > 250 MeV, similar to those predicted in Ref. [27], which can be considered to be due to the supershort mode. A few events can also be observed in Fig. 3(d) corresponding to ^{256}Fm but a better statistics may be required to confirm the presence of the supershort mode. Therefore, the experimental observation of the onset of the supershort mode of fission can be considered to be from ^{257}Md .

The width of the measured TKE distribution σ_{TKE} as a function of excitation energy has been compared for different systems (symbols) along with the GEF version 2020/1.1 [37] model predictions (lines), as shown in Fig. 4. It can be observed that the average σ_{TKE} for ^{257}Md is much larger compared with ^{251}Es as well as the calculations, which may be a confirmatory signature of the presence of the supershort mode. A difference between the experimental data even for ^{251}Es and GEF predictions can be understood in terms of the broadening in mass and velocity resolutions.

The projections of the above 2D correlation plots onto the mass axis that provide the mass distributions are shown in Figs. 5(a)–5(f). The mass distributions of FF from the ^{257}Md nucleus could be fit the best by using three Gaussian distributions: two of which represent standard asymmetric modes and the third one peaking at $A_{\text{CN}}/2$ representing symmetric

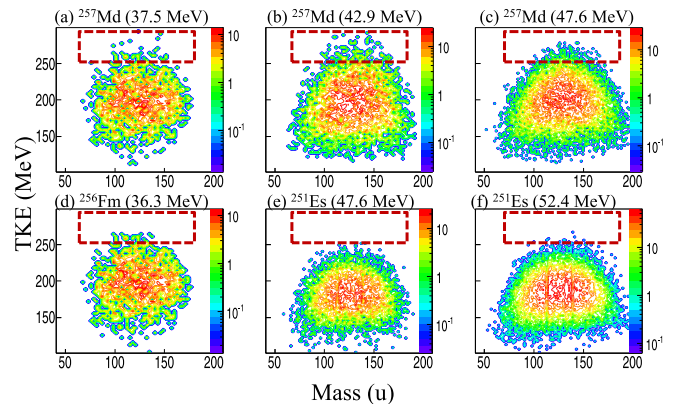


FIG. 3. Mass-TKE correlations obtained from the fissioning nucleus (a)–(c) ^{257}Md , (d) ^{256}Fm , and (e), (f) ^{251}Es . The events within the dotted rectangles, with higher TKE, are likely to be due to the supershort mode of fission.

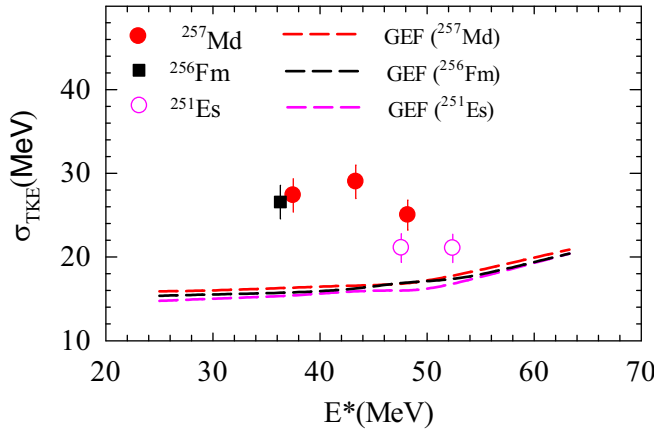


FIG. 4. Comparison of the widths σ_{TKE} of the measured TKE-distributions for the fissioning nuclei ^{257}Md , ^{256}Fm , and ^{251}Es along with the GEF predictions (lines).

distributions that include both superlong as well as super-short modes. However, the remaining distributions shown in Figs. 5(d)–5(f) corresponding to ^{256}Fm and ^{251}Es nuclei which were also fit with three Gaussian functions, the Gaussian function peaking at $A_{\text{CN}}/2$ represents only the superlong mode. It may be mentioned that, out of two Gaussian distributions representing an asymmetric mode, one was peaking at 143–145 u, which is again a confirmatory nature of asymmetric fission of actinides. It is also important to mention that such an asymmetric mode at the present excitation energy range is not expected unless we invoke the concept of multichance fission, the effect of which in FF mass distributions have been discussed in Ref. [19].

Furthermore, from the fitting of total TKE distributions described earlier, one can obtain the contributions of low-TKE and high-TKE modes from the ^{257}Md nucleus. It may be recollected that the high-TKE mode represents the supershort

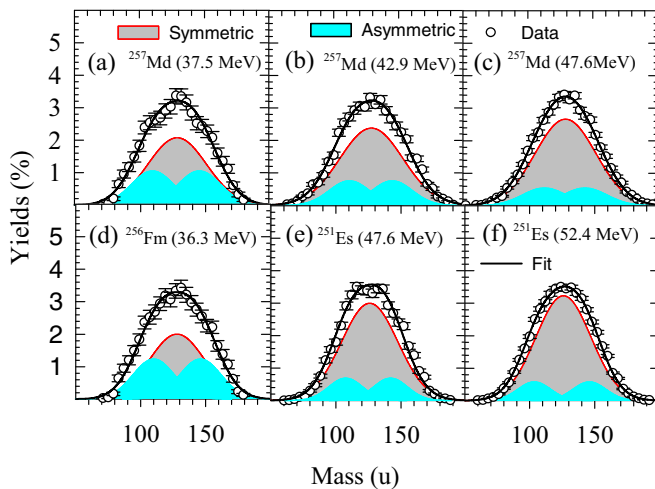


FIG. 5. Mass-distributions obtained from the fissioning nucleus (a)–(c) ^{257}Md , (d) ^{256}Fm , and (e), (f) ^{251}Es . The contributions from symmetric and asymmetric modes are shown by filled gray and cyan regions, respectively.

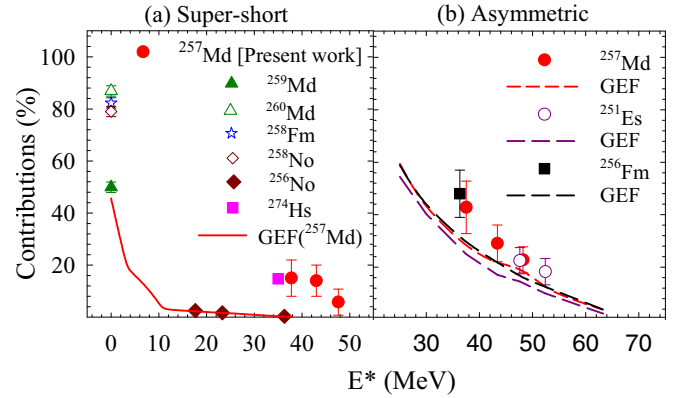


FIG. 6. (a) Comparison of contributions from the supershort mode for the present nucleus ^{257}Md with the available literature data (symbols) and GEF calculations (solid line). (b) Comparison of determined contributions from the asymmetric mode (symbols) with the GEF calculation (dashed lines) for each nucleus populated in the present experiment.

mode, whereas the low-TKE mode could be comprised of both the standard asymmetric and the superlong modes of fission. Therefore, contributions from the supershort mode can be determined from the fitting of the TKE distributions. In contrast, contributions from the other two modes could be determined from the fitting of FF mass distributions. Thus, the contribution from the supershort mode for the ^{257}Md nucleus as a function of excitation energy has been compared with the available literature data in Fig. 6(a), where it can be observed that the supershort mode is very dominant in spontaneous fission from ^{259}Md (filled triangles), ^{260}Md (hollow triangles), ^{258}Fm (hollow stars), and ^{258}No (hollow diamonds), which is not very surprising due to the strong shell effect at zero excitation energy. Furthermore, it can be observed that, for the ^{256}No nucleus (filled diamonds), the contribution from the supershort mode gradually decreases from 3.0% to 0.3% as excitation energy increases from 17 to 35 MeV. Similarly, for the ^{274}Hs nucleus (filled squares), the contribution at $E^* \approx 35$ MeV is $\approx 17\%$, which completely vanishes for $E^* = 48$ MeV. However, for the present system it is interesting to find that the contribution is nonzero at $E^* = 43$ as well as 48 MeV. To understand the experimental observation, the contribution from the supershort mode for the ^{257}Md nucleus has also been calculated using the semi-empirical model code GEF [37] and compared with the present systematics, as shown in Fig. 6(a). It can be observed that the theoretical predictions for $E^* > 30$ MeV is almost zero, a huge underprediction with respect to the observed values. On the other hand, the contributions from the standard asymmetric mode from ^{257}Md , ^{251}Es , and ^{256}Fm , as shown in Fig. 6(b), are found to be comparable to the results obtained from the GEF code.

It is important to discuss here that the origin of the standard asymmetric mode and the supershort mode is the shell effect in the fragment nuclei. It is now well known [38–41] that the fragment nucleus responsible for the standard asymmetric fission is the nucleus with $Z \approx 56$ and $A \approx 142$ and for the other mode is the two doubly magic nuclei ^{132}Sn . The shell

effect always increases the binding energy of the system in the corresponding valley. It is important to mention that the shell correction energy at zero temperature for the supershort mode is larger than those for the standard asymmetric mode. Apparently, the shell effect could be stronger for the supershort mode than the asymmetric mode even at high excitation energy. But a large part of the gain in binding energy in the supershort mode must be paid to compensate the larger Coulomb repulsion (compared with the asymmetric mode) between the nascent fragments in this compact configuration, and the shell effect vanishes much faster than the standard asymmetric mode. From the model calculations it is learned that contribution from the supershort mode is negligibly small at $E^* > 30$ MeV, whereas contributions from the asymmetric mode from a single fissioning nucleus could be significant at $E^* > 30$ MeV. Due to the presaddle neutron evaporations, the fissioning system gets cooled down to acquire low excitation energy, thereby revealing more microscopic effects in the measured mass and TKE distributions. Thus, the contributions from multichance fission makes the asymmetric mode stronger, as can be observed from the present data also. The model calculations by GEF are supposed to take care of this effect. However, the discrepancy between the experimental observation and the theoretical calculations on the contributions of the supershort mode at higher excitation energies highlights the need for a better understanding of these rare fission modes for neutron-rich nuclei.

In summary, the mass and TKE distributions of fission fragments from the ^{257}Md nucleus formed by complete fusion in the $^{19}\text{F} + ^{238}\text{U}$ reaction were measured over the excitation energy range $E^* \approx 37\text{--}48$ MeV. The shape of the TKE distributions are found to be of skewed Gaussian whose explanation requires two Gaussian functions with centroid energies of ≈ 193 and 230 MeV. The peak energy of the low-TKE component is consistent with the Viola systematics but the high-TKE component seems to originate from the supershort

mode of fission. To confirm this, two more measurements have been carried out for $^{19}\text{F} + ^{232}\text{Th}$ and $^{18}\text{O} + ^{238}\text{U}$ reactions involving first a different target and then a different projectile, leading to compound nuclei ^{251}Es and ^{256}Fm , respectively, at similar excitation energies. A comparison of the mass-TKE correlation plots and the TKE widths for the three systems confirms the presence of the supershort mode for the ^{257}Md nucleus, which is absent for the ^{251}Es and ^{256}Fm compound nuclei.

The FF mass distributions, obtained for all the cases, have been fit by using three Gaussian functions, two of which represent the asymmetric mode and the third one representing the symmetric mode. The presence of asymmetric fission has been attributed to the cooling of the compound nuclei due to multichance fission. Contributions from supershort mode and asymmetric mode obtained from the fit to the TKE distributions and mass-distribution, respectively, have been compared with the predictions by the semi-empirical model code GEF. Although the GEF prediction for the asymmetric component reasonably reproduces the experimental data, it underpredicts the contribution of the supershort mode obtained from the experimental data by a large factor.

The present work provides a new experimental observation on the existence of the supershort mode of fission in the ^{257}Md nucleus. This nucleus is a new inclusion in the nuclear chart in the mass region of $A \approx 260$, where some of the nuclei exhibit the supershort mode in spontaneous or low-energy fission. It may be emphasized that the existence of the supershort mode up to the excitation energy of ≈ 48 MeV, observed for the first time, is quite interesting and it highlights the lack of complete understanding in such fission modes in exotic nuclei and the inadequacy of the liquid drop model, even at high excitation energy.

Fruitful discussions with K.-H. Schmidt during the preparation of the paper are acknowledged.

-
- [1] Y. Oganessian and V. Utyonkov, *Rep. Prog. Phys.* **78**, 036301 (2015).
- [2] S. A. Giuliani, Z. Matheson, W. Nazarewicz, E. Olsen, P.-G. Reinhard, J. Sadhukhan, B. Schuetrumpf, N. Schunck, and P. Schwerdtfeger, *Rev. Mod. Phys.* **91**, 011001 (2019).
- [3] S. A. Giuliani, G. Martínez-Pinedo, and L. M. Robledo, *Phys. Rev. C* **97**, 034323 (2018).
- [4] S. Goriely, J.-L. Sida, J.-F. Lemaître, S. Panebianco, N. Dubray, S. Hilaire, A. Bauswein, and H.-T. Janka, *Phys. Rev. Lett.* **111**, 242502 (2013).
- [5] S. Santra, A. Pal, P. K. Rath, B. K. Nayak, N. L. Singh, D. Chattopadhyay, B. R. Behera, V. Singh, A. Jhingan, P. Sugathan, K. S. Golda, S. Sodaye, S. Appannababu, E. Prasad, and S. Kailas, *Phys. Rev. C* **90**, 064620 (2014).
- [6] R. Yanez, D. J. Hinde, B. Bouriquet, and D. Duniec, *Phys. Rev. C* **71**, 041602(R) (2005).
- [7] M. Itkis, J. Aysto, S. Beghini, A. Bogachev, L. Corradi, O. Dorvaux, A. Gadea, G. Giardina, F. Hanappe, I. M. Itkis, M. Jandel, J. Kliman, S. V. Khlebnikov, G. N. Kniajeva, N. A. Kondratiev, E. M. Kozulin, L. Krupa, A. Latina, T. Materna, G. Montagnoli *et al.*, *Nucl. Phys. A* **734**, 136 (2004).
- [8] T. K. Ghosh, K. Banerjee, C. Bhattacharya, S. Bhattacharya, S. Kundu, P. Mali, J. K. Meena, G. Mukherjee, S. Mukhopadhyay, T. K. Rana, P. Bhattacharya, and K. S. Golda, *Phys. Rev. C* **79**, 054607 (2009).
- [9] K. Banerjee, T. K. Ghosh, S. Bhattacharya, C. Bhattacharya, S. Kundu, T. K. Rana, G. Mukherjee, J. K. Meena, J. Sadhukhan, S. Pal, P. Bhattacharya, K. S. Golda, P. Sugathan, and R. P. Singh, *Phys. Rev. C* **83**, 024605 (2011).
- [10] T. K. Ghosh, S. Pal, T. Sinha, S. Chattopadhyay, P. Bhattacharya, D. C. Biswas, and K. S. Golda, *Phys. Rev. C* **70**, 011604(R) (2004).
- [11] D. J. Hinde, M. Dasgupta, J. R. Leigh, J. P. Lestone, J. C. Mein, C. R. Morton, J. O. Newton, and H. Timmers, *Phys. Rev. Lett.* **74**, 1295 (1995).
- [12] R. Rafiei, R. G. Thomas, D. J. Hinde, M. Dasgupta, C. R. Morton, L. R. Gasques, M. L. Brown, and M. D. Rodriguez, *Phys. Rev. C* **77**, 024606 (2008).

- [13] M. G. Itkis, E. Vardaci, I. M. Itkis, G. N. Knyazheva, and E. M. Kozulin, *Nucl. Phys. A* **944**, 204 (2015).
- [14] A. Andreyev, J. Elseviers, M. Huyse, P. V. Duppen, S. Antalic, A. Barzakh, N. Bree, T. E. Cocolios, V. F. Comas, J. Diriken, D. Fedorov, V. Fedosseev, S. Franchoo, J. A. Heredia, O. Ivanov, U. Koster, B. A. Marsh, P. Van den Bergh, J. Van De Walle, K. Nishio *et al.*, *Phys. Rev. Lett.* **105**, 252502 (2010).
- [15] A. Chatillon, J. Taieb, H. Alvarez-Pol, L. Audouin, Y. Ayyad, G. Bélier, J. Benlliure, G. Boutoux, M. Caamano, E. Casarejos, D. Cortina-Gil, A. Ebran, F. Farget, B. Fernandez-Dominguez, T. Gorbinet, L. Grente, A. Heinz, H. T. Johansson, B. Jurado, A. Kelic-Heil, N. Kurz, B. Laurent *et al.*, *Phys. Rev. Lett.* **124**, 202502 (2020).
- [16] C. Schmitt, A. Lemasson, K.-H. Schmidt, A. Jhingan, S. Biswas, Y. H. Kim, D. Ramos, A. N. Andreyev, D. Curien, M. Ciemala, E. Clement, O. Dorvaux, B. De Canditiis, F. Didierjean, G. Duchene, J. Dudouet, J. Frankland, B. Jacquot, C. Raison, D. Ralet *et al.*, *Phys. Rev. Lett.* **126**, 132502 (2021).
- [17] R. Léguillon, K. Nishio, K. Hirose, H. Maki, I. Nishinaka, R. Orlandia, K. Tsukada, J. Smallcombe, S. Chiba, Y. Aritomod, T. Ohtsuki, R. Tatsuzawa, N. Takaki, N. Tamura, S. Goto, I. Tsekhanovich, C. M. Petrache, A. N. Andreyev, *Phys. Lett. B* **761**, 125 (2016).
- [18] D. Ramos, M. Caamano, F. Farget, C. Rodriguez-Tajes, L. Audouin, J. Benlliure, E. Casarejos, E. Clement, D. Cortina, O. Delaune, X. Derkx, A. Dijon, D. Dore, B. Fernandez-Dominguez, G. de France, A. Heinz, B. Jacquot, A. Navin, C. Paradela, M. Rejmund, T. Roger, M.-D. Salsac, and C. Schmitt, *Phys. Rev. C* **97**, 054612 (2018).
- [19] K. Hirose, K. Nishio, S. Tanaka, R. Leguillon, H. Makii, I. Nishinaka, R. Orlandi, K. Tsukada, J. Smallcombe, M. J. Vermeulen, S. Chiba, Y. Aritomo, T. Ohtsuki, K. Nakano, S. Araki, Y. Watanabe, R. Tatsuzawa, N. Takaki, N. Tamura, S. Goto, I. Tsekhanovich, and A. N. Andreyev, *Phys. Rev. Lett.* **119**, 222501 (2017).
- [20] A. Pal, S. Santra, D. Chattopadhyay, A. Kundu, A. Jhingan, P. Sugathan, N. Saneesh, M. Kumar, N. L. Singh, A. Yadav, C. Yadav, R. Dubey, K. Kapoor, K. Rani, H. Arora, A. C. Visakh, D. Kaur, B. K. Nayak, A. Saxena, S. Kailas, and K.-H. Schmidt, *Phys. Rev. C* **98**, 031601(R) (2018).
- [21] M. Itkis, V. Okolovich, A. Russanov, and G. Smirenkin, *Z. Phys. A: At. Nucl.* (1975) **320**, 433 (1985).
- [22] I. V. Pokrovsky, L. Calabretta, M. G. Itkis, N. A. Kondratiev, E. M. Kozulin, C. Maiolino, E. V. Prokhorova, A. Y. Rusanov, and S. P. Tretyakova, *Phys. Rev. C* **60**, 041304(R) (1999).
- [23] I. V. Pokrovsky, M. G. Itkis, J. M. Itkis, N. A. Kondratiev, E. M. Kozulin, E. V. Prokhorova, V. S. Salamatina, V. V. Pashkevich, S. I. Mulgin, A. Y. Rusanov, S. V. Zhdanov, G. G. Chubarian, B. J. Hurst, R. P. Schmitt, C. Agodi, G. Bellia, L. Calabretta, K. Lukashin, C. Maiolino, A. Kelic, G. Rudolf, L. Stuttge, and F. Hanappe, *Phys. Rev. C* **62**, 014615 (2000).
- [24] H. Britt, H. Wegner, and J. Gursky, *Phys. Rev.* **129**, 2239 (1963).
- [25] E. K. Hulet, J. F. Wild, R. J. Dougan, R. W. Loughheed, J. H. Landrum, A. D. Dougan, M. Schadel, R. L. Hahn, P. A. Baisden, C. M. Henderson, R. J. Dupzyk, K. Summerer, and G. R. Bethune, *Phys. Rev. Lett.* **56**, 313 (1986).
- [26] E. K. Hulet, J. F. Wild, R. J. Dougan, R. W. Loughheed, J. H. Landrum, A. D. Dougan, P. A. Baisden, C. M. Henderson, R. J. Dupzyk, R. L. Hahn, M. Schadel, K. Summerer, and G. R. Bethune, *Phys. Rev. C* **40**, 770 (1989).
- [27] M. D. Usang, F. A. Ivanyuk, C. Ishizuka, and S. Chiba, *Sci. Rep.* **9**, 1525 (2019).
- [28] S. N. Dmitriev, Y. Ts. Oganessyan, V. K. Utyonkov, S. V. Shishkin, A. V. Yeremin, Y. V. Lobanov, Y. S. Tsyganov, V. I. Chepygin, E. A. Sokol, G. K. Vostokin, N. V. Aksenov, M. Hussonnois, M. G. Itkis, H. W. Gäggeler, D. Schumann, H. Bruchertseifer, R. Eichler, D. A. Shaughnessy, P. A. Wilk, J. M. Kenneally, M. A. Stoyerd and J. F. Wild, *Mendelevov Commun.* **15**, 1 (2005).
- [29] Y. Ts. Oganessian, *J. Phys. G* **34**, R165 (2007).
- [30] I. M. Itkis, E. M. Kozulin, M. G. Itkis, G. N. Knyazheva, A. A. Bogachev, E. V. Chernysheva, L. Krupa, Y. T. Oganessian, V. I. Zagrebaev, A. Y. Rusanov, F. Goennenwein, O. Dorvaux, L. Stuttge, F. Hanappe, E. Vardaci, and E. de Goes Brennand, *Phys. Rev. C* **83**, 064613 (2011).
- [31] K. F. Flynn, E. P. Horwitz, C. A. A. Bloomquist, R. F. Barnes, R. K. Sjoblom, P. R. Fields, and L. E. Glendenin, *Phys. Rev. C* **5**, 1725 (1972).
- [32] E. Prokhorova, A. Bogachev, M. Itkis, I. Itkis, G. Knyazheva, N. Kondratiev, E. Kozulin, L. Krupa, Y. Oganessian, I. Pokrovsky, L. Krupa, Yu. Ts. Oganessian, I. V. Pokrovsky, V. V. Pashkevich, and A. Ya. Rusanov, *Nucl. Phys. A* **802**, 45 (2008).
- [33] A. Pal, S. Santra, A. Kundu, D. Chattopadhyay, A. Jhingan, B. Nayak, and S. Prafulla, *J. Instrum.* **15**, P02008 (2020).
- [34] R. G. Thomas, D. J. Hinde, D. Duniec, F. Zenke, M. Dasgupta, M. L. Brown, M. Evers, L. R. Gasques, M. D. Rodriguez, and A. Diaz-Torres, *Phys. Rev. C* **77**, 034610 (2008).
- [35] J. Ziegler, Computer code SRIM (2013).
- [36] V. E. Viola, K. Kwiatkowski, and M. Walker, *Phys. Rev. C* **31**, 1550 (1985).
- [37] K.-H. Schmidt, B. Jurado, C. Amouroux, and C. Schmitt, *Nucl. Data Sheets* **131**, 107 (2016).
- [38] C. Bockstiegel, S. Steinhauser, K. H. Schmidt, H.-G. Clerc, A. Grewe, A. Heinz, M. de Jong, A. R. Junghans, J. Muller, and B. Voss, *Nucl. Phys. A* **802**, 12 (2008).
- [39] K. H. Schmidt, S. Steinhauser, C. Bockstiegel, A. Grewe, A. Heinz, A. R. Junghans, J. Benlliure, H.-G. Clerc, M. de Jong, J. Muller, M. Pfitzner, and B. Voss, *Nucl. Phys. A* **665**, 221 (2000).
- [40] G. Scamps and C. Simenel, *Nature (London)* **564**, 382 (2018).
- [41] D. Ramos, M. Caamano, A. Lemasson, M. Rejmund, L. Audouin, H. Alvarez-Pol, J. D. Frankland, B. Fernandez-Dominguez, E. Galiana-Baldo, J. Piot, D. Ackermann, S. Biswas, E. Clement, D. Durand, F. Farget, M. O. Fregeau, D. Galaviz, A. Heinz, A. I. Henriques, B. Jacquot, B. Jurado, Y. H. Kim, P. Morfouace, D. Ralet, T. Roger, C. Schmitt, P. Teubig, and I. Tsekhanovich, *Phys. Rev. Lett.* **123**, 092503 (2019).